TECHNIQUES

3D Imaging, Registration, and Analysis of the Early Mouse Embryonic Vasculature

Gregory A. Anderson,[1,2]* Michael D. Wong,[1,2] Jian Yang,[2] and R. Mark Henkelman[1,2]

Background: Cardiovascular development requires the input of a large number of molecular signaling molecules, and undergoes tightly regulated, three-dimensional developmental patterning. Conventional developmental biology techniques have successfully identified many of the signaling cascades and molecular cues necessary for proper cardiovascular development, which has furnished us with a wealth of biochemical, molecular, and biologically functional information on how tightly linked cardiac and vascular development are. Still missing, however, is a genuine appreciation of the three-dimensional (3D) nature of these important developmental steps. Results: Optical projection tomography (OPT) is a 3D imaging technique that allows for high-resolution imaging of early mouse embryos and their developing cardiovascular systems when a PECAM-1 antibody stain is used to highlight the vascular branching. Reported here is a method in which several 3D images of mouse embryo vasculatures can be registered, thus allowing for analysis of within-strain variance between genetically identical mouse pups. Post-registration, small differences in somitogenesis and ventricular trabeculation patterning can be visualized in mouse pups that differ by as little as a few hours of gestational time. Additionally, similarity metrics (cross-correlation values) can be calculated to quantify similarities and differences. Two different mouse strains are analyzed (C57Bl/6 and CD-1), and similar results are recognized in each strain. Conclusions: Visualizing the cardiovascular system in such a precise 3D manner allows for more accuracy in describing the steps that take place during cardiovascular development. This novel method will be applicable to many developmental biology questions in other organ systems and other species. *Developmental Dynamics 242:527–538, 2013.*

Key words: optical projection tomography; heart development; developmental biology; vascular biology; embryo staining

Key findings:

- Conventional developmental biology techniques do not allow for a full appreciation of the 3D nature of cardiovascular development.
- Mouse embryo populations imaged by optical projection tomography (OPT) and subsequently registered together in 3D allow for the comparison of vascular maps of individual mice.
- Small developmental differences in both blood vessel and cardiac development are distinguishable in mouse embryos that differ by as little as a few hours of gestational time.

Accepted 7 February 2013

ABBREVIATIONS USED: Micro-CT, micro-computed tomography; MIP, maximum intensity projection; MRI, magnetic resonance imaging; OPT, optical projection tomography; RMS, root mean square.

[1]Department of Medical Biophysics, University of Toronto, Toronto, Canada
[2]Mouse Imaging Centre, The Hospital For Sick Children, Toronto, Canada
Grant sponsor: Ontario Research Fund.
***Correspondence to: Gregory A. Anderson, Mouse Imaging Centre, The Hospital For Sick Children, 25 Orde Street, Toronto, Ontario, Canada M5T 3H7. E-mail: ganderson@phenogenomics.ca**

DOI: 10.1002/dvdy.23947
Published online 15 February 2013 in Wiley Online Library (wileyonlinelibrary.com).

Developmental Dynamics

INTRODUCTION

Cardiovascular development is a sublimely complicated process that involves precise timing of a multitude of molecular events, and a myriad of subtle three-dimensional conformational changes. Traditional developmental biology techniques have been used extensively to detail cardiovascular development in the mouse, as well as non-mammalian species including zebrafish (Isogai et al., 2001, 2003) and chick (Coffin and Poole, 1988; Poole and Coffin, 1989), providing vast quantities of qualitative knowledge as to how these complex organ systems develop. However, the major drawback of current developmental biological imaging is that it is two-dimensional (2D) in nature. Thus, a full understanding of how blood vessels track in three-dimensional (3D) space during development is not fully appreciated, nor is it clear how tightly controlled vascular patterning events are between different developing individuals. What is crucially needed is a method to both characterize and co-localize, in three-dimensional space, the vasculatures of a population of genetically identical mice. This will enable the generation of average vascular maps of the growing arborized blood vessel trees of populations of mice, but will also allow for the identification of small differences in cardiovascular development at discrete developmental time points of the different individuals within the population. Similar methods have been described for the *Drosophila* adult brain vasculature (Peng et al., 2011), which has a tightly regulated vascular pattern, but to our knowledge this has not been described for whole mount mammalian specimens.

Optical projection tomography (OPT) is a powerful imaging modality that is ideally suited to visualize the complex three-dimensional structure of the mouse embryo. We have shown that we can image early mouse embryos at high resolution to obtain 3D images of their developing vasculature (Walls et al., 2008), and, furthermore, that we can detect cardiovascular abnormalities in mutant mouse models (Lickert et al., 2004). But OPT has far more potential than simply being a tool to generate elegant 3D pictures; the digital nature of data collected by OPT allows it to be used for quantitative analysis. Since it is well known that using a population of mice rather than one individual allows for the capture of within-strain developmental variance (Zamyadi et al., 2010; Wong et al., 2012b), presented here is a similar method of vascular registration for early mouse embryos. Autofluorescence (for general anatomy) and vascular-specific PECAM-1 OPT scans of several mouse embryos within two different background strains are collected at specific developmental time points. PECAM-1, the major constituent of the endothelial cell intercellular junction, has been extensively used as a molecular marker of mature endothelial cells (Drake and Fleming, 2000; Gerety and Anderson, 2002; Chaturvedi and Sarkar, 2006; Suchting et al., 2007), and thus identifies the growing vascular tree. Using autofluorescence scans as an initial guide, individual mouse vasculature images are then co-registered in three-dimensional space, thus superimposing the datasets to create a population average image of all samples. Once fully registered in 3D, the similarities and differences between each individual vascular map at homologous points in anatomy can be visualized. This allows for the investigation of temporal differences in cardiovascular development of specific embryos at discrete developmental time points, and will allow for the mapping of developmental differences caused by genetic mutations as well.

Here we outline a novel method for registering the vasculatures of several mouse embryos into a common three-dimensional space, which allows for comparisons of high-resolution vascular structures. Whether they come from a C57Bl/6 or CD-1 background, embryos at a specific developmental stage have vascular maps that are both rapidly patterned and tightly controlled; embryos that differ by as little as one to three somites have small developmental differences in their vasculature that can be visualized. The ability to visualize such precise developmental processes of the cardiovascular system allows for more accuracy in identifying and describing the steps that take place during this complex process, and provides more information about the individual genetic and hemodynamic requirements necessary to create a functional mammalian heart and vascular network. This method will be amenable to many developmental biology questions in both other organ systems and other species, and will be of great use in future studies of genetically modified organisms.

RESULTS

Acquisition of OPT Data and Comparison With Histology

OPT was developed to fill a need for 3D cellular resolution imaging of biological specimens that are up to a few cubic centimeters in size (Sharpe et al., 2002). Its ability to support the use of molecular markers such as PECAM-1, and other endothelial cell-specific markers (Drake and Fleming, 2000), makes it an extremely valuable tool for the study of mouse cardiovascular development, since the growing vasculature can be imaged at early developmental stages, anywhere from 5 to 30 somites (Walls et al., 2008). Our in-house built OPT system (Fig. 1A and B) (Wong et al., 2012a) was used to capture projection images of mouse PECAM-stained embryos, which were then reconstructed using a standard parallel ray filtered back-projection reconstruction algorithm, which resulted in 3D datasets that can be manipulated, digitally sliced, and viewed from any angle (Slaney and Kak, 1988). Figure 1 illustrates the high-resolution data that OPT is capable of producing when imaging a 21-somite C57Bl/6 embryo. Autofluorescence data is acquired using GFP excitation and emission filters to capture the intrinsic signal of all tissues, thus supplying us with general anatomical information (Fig. 1C–F). Vascular data are acquired using Cy3 excitation and emission filters to capture the PECAM-1 signal of endothelial cells, thus supplying us with vascular anatomy information (Fig. 1C'–F'). Due to the digital nature of the data and its simultaneous acquisition, dual channel images of both the autofluorescence and vascular data can be obtained (Fig. 1C"–F"),

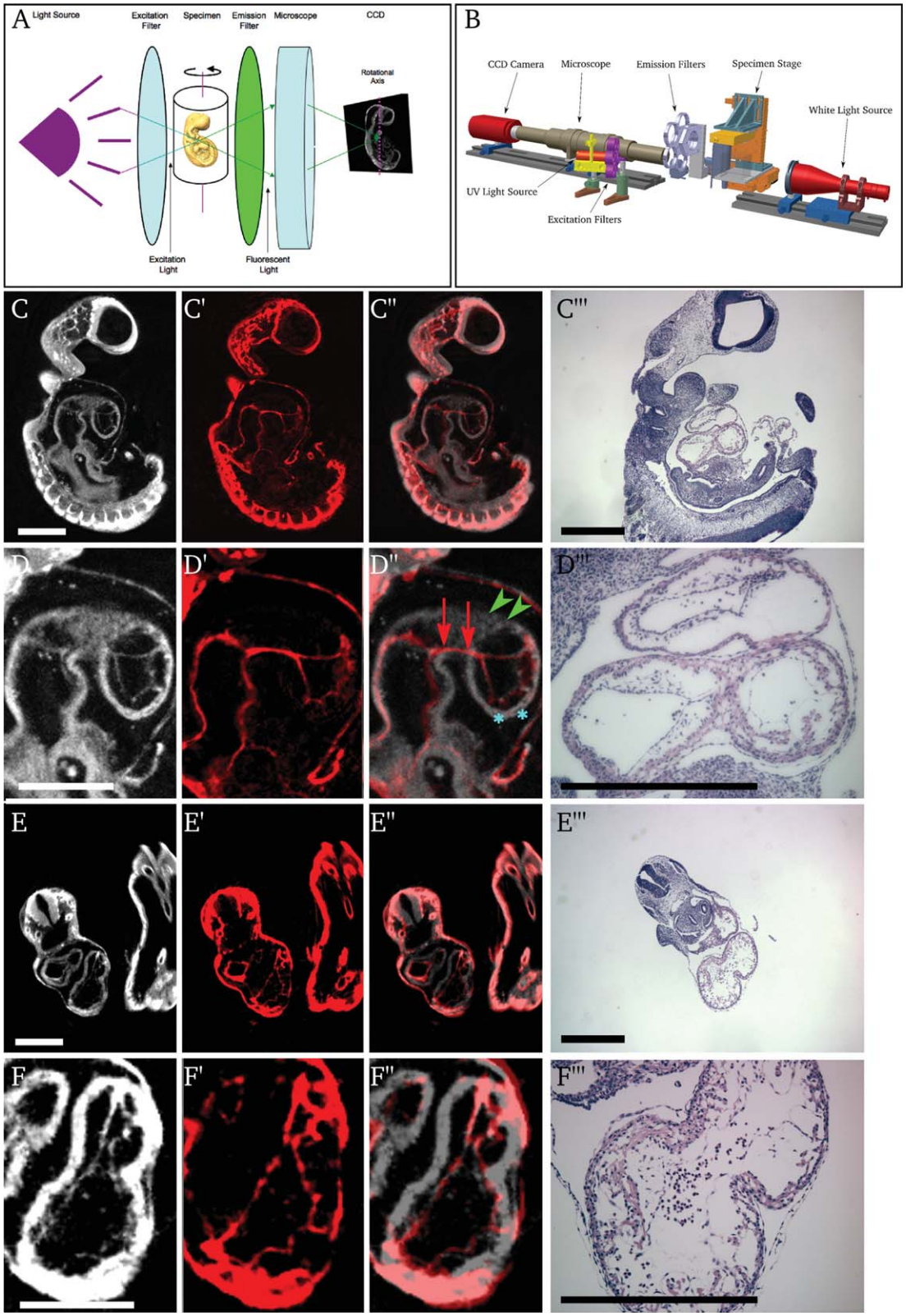

Fig. 1. Acquisition of OPT data and comparison with histology. **A:** The general OPT acquisition setup in cartoon form to illustrate the acquisition process. **B:** A schematic of the in-house built OPT system. Autofluorescence data of a 21-somite embryo is collected using an autofluorescence filter set, and is shown in sagittal sections (**C**, and as an enlarged region of interest in **D**), or in transverse sections (**E**, and as an enlarged region of interest in **F**) to illustrate the development of the heart at this developmental time point. The comparative vascular data of the embryo is collected using a Cy3 filter set, and the same slices are shown in sagittal sections (**C',D'**) or transverse sections (**E',F'**). The data, when overlapped, show that the vasculature precisely aligns with the autofluorescence data in both sagittal (**C",D"**) and transverse (**E",F"**) views, and that the PECAM staining is specific (the red arrows in D" point out the specific endothelial cell staining of the atrioventricular canal, the blue asterisks indicate the ventricular trabeculations, while the green arrowheads point to the myocardial tissue has not been stained with PECAM-1). In order to appreciate more fully the 3D nature of the data, all images are an average image of a 5-slice stack, thus corresponding to a 27.5-μm slab. Shown for comparison are comparative histological sections of a littermate control embryo (**C'"–F'"**). Scale bars = 500 μm.

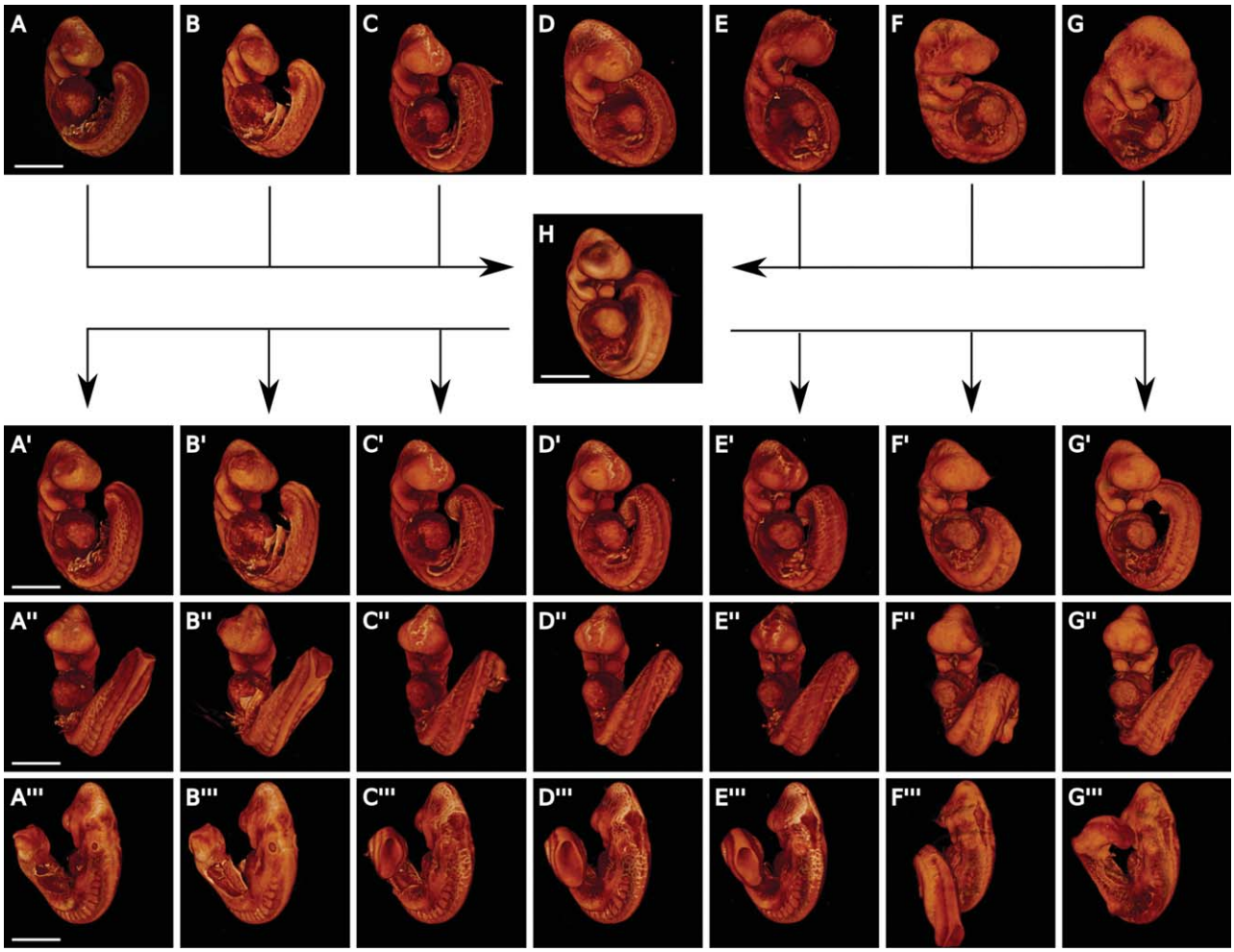

Fig. 2. Autofluorescence registration of seven E9.5 embryos. Autofluorescence scans of the embryos (**A–G**) are used for the first stage of the registration process (see Experimental Procedures section). Following both linear/affine and non-linear registration, a population average of the seven embryos is generated (**H**), which represents the global anatomy of the embryos. All of the registration steps necessary to reach the population average are then applied to each individual embryo to see how each embryo has changed (**A'–G', A"–G", A'"–G'"**; shown in three different orientations). All data can be fully manipulated in 3D. Scale bars = 500 μm.

illustrating where the blood vessels reside in relation to the tissue as a whole. Sagittal (Fig. 1C–C", D–D"), transverse (Fig. 1E–E", F–F"), coronal/frontal (data not shown), as well as arbitrary oblique sections can be viewed as desired, in order to characterize organs such as the growing heart or the budding intersomitic blood vessels in their most beneficial orientation. Figure 1D", for instance, illustrates the atrioventricular canal and the endocardial cushions of the developing heart (red arrows). Additionally, the trabeculations of the ventricle are visible due to the PECAM-1 stain (blue asterisks). The PECAM-1 stain is specific to the endocardium of the heart, as illustrated by the fact that the myocardium is not stained (green arrowheads). Similar observations can be made from the paired transverse sections of the same embryo (Fig. 1F"). Histological sections of a littermate control embryo (Fig. 1C'"–F'") are shown for comparison.

Registration of Seven E9.5 Embryos

Registration is a process that attempts to manipulate two or more 3D datasets into a common 3D space, so that similarities and differences between individual samples at equivalent locations can be recognized. This has been used to great success in neuroanatomy studies (Spring et al., 2007; Dorr et al., 2008; Lerch et al., 2008). It has recently been applied to mouse embryo studies of general anatomy, though this work has tended to focus on older, larger embryos that have been imaged using magnetic resonance imaging (MRI) (Zamyadi et al., 2010; Cleary et al., 2011) or micro-computed tomography (micro-CT) (Wong et al., 2012b). The embryo registration method employed here is based upon the current mouse brain registration algorithm employed in our laboratory (Kovacevic et al., 2005), but has been modified with additional steps to make it sensitive to the very fine features of the mouse embryonic vasculature. We first looked at C57Bl/6 embryos. We collected autofluorescence and vascular OPT scans of somite stage–matched embryos (20–23 somites; n=7). During the registration algorithm, the autofluorescence data

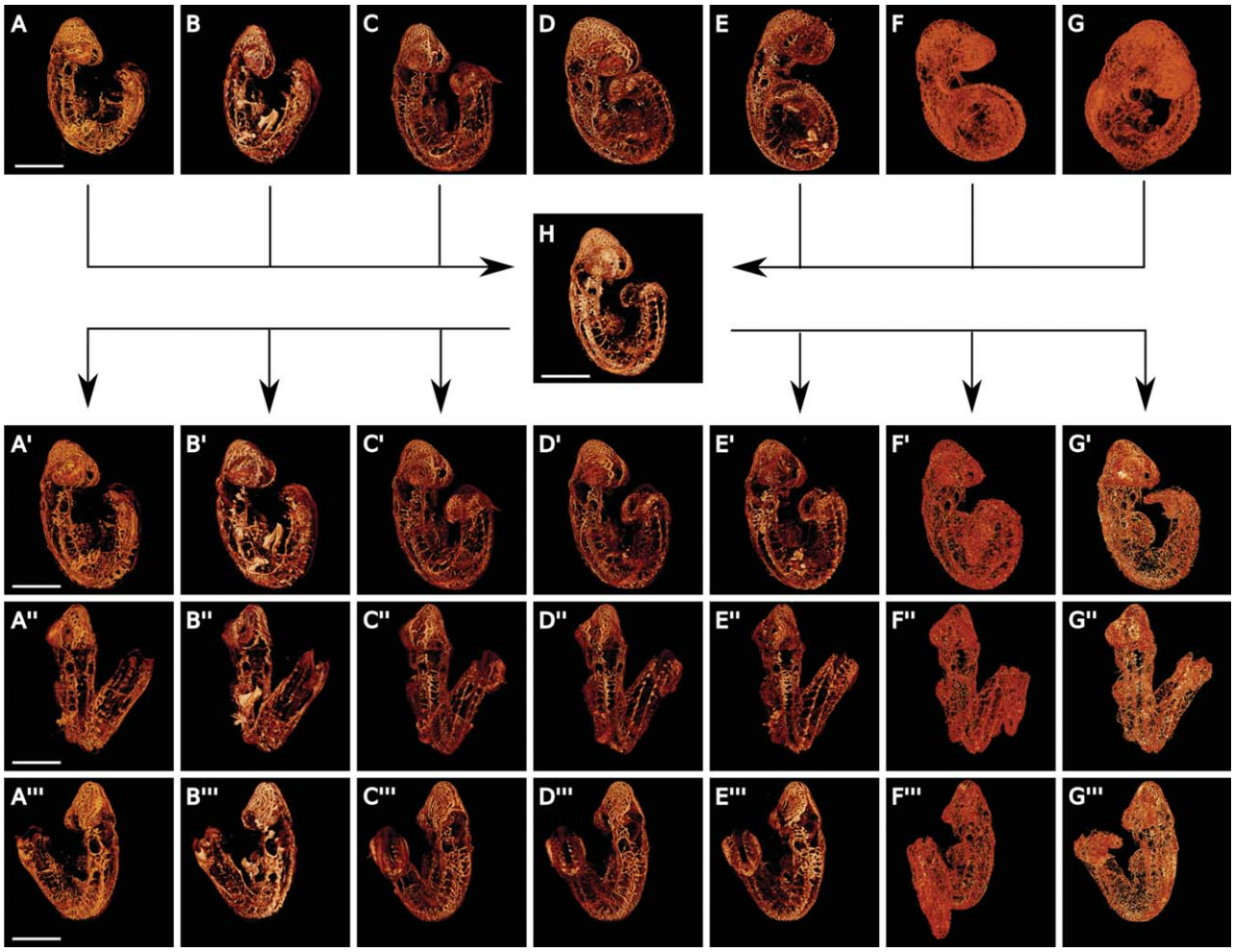

Fig. 3. Vascular tree registration of seven E9.5 embryos. Following registration of the global anatomy, the original vascular scans of each respective embryo (**A–G**) are then subjected to the deformation field produced by the registration of the autofluorescence data, followed by further non-linear registration steps in order to account for small residual differences in the vascular scan data (see Experimental Procedures section), which again generates a population average vasculature image of the embryos (**H**). The registration steps generated in this process to reach the population average can once again be applied to the original vascular scan data in order to visualize the vascular patterns of each individual embryo in equivalent orientations (**A'–G', A"–G", A"'–G"'**; shown in three different orientations). All data can be fully manipulated in 3D. Scale bars = 500 μm.

(Fig. 2A–G, represented as volume textured samples) are first used to register the embryos together, where first a set of 3D affine transformations (translations, rotations, scaling factors, and shearing factors), and secondly non-linear, voxel-by-voxel transformations are used to generate a representative consensus average image of all embryo inputs (Fig. 2H). These transformations are encoded in a deformation field for each 3D input image, which, when applied to the original autofluorescence image of each embryo, result in registered images that look very similar (Fig. 2A'–G', A"–G", and A"'–G"', shown in three orientations). The corresponding deformation fields are then applied to the vascular scans of the individual embryos (Fig. 3A–G, represented as volume-textured images in their original orientations), which approximately registers the individual vascular trees together. However, since the vascular structures are so fine, there are evident registration mismatches (data not shown). Therefore, the vascular images are then subjected to an additional registration algorithm that consists of another set of non-linear, voxel-by-voxel transformations. Thus, a representative consensus average of all vascular maps is calculated (Fig. 3H), and the same process as previously described results in registered vasculature images that look very similar (Fig. 3A'–G', A"–G", A"'–G"', shown in three orientations).

We next performed the same procedure on a set of somite stage–matched mouse embryos on the CD-1 background (20–23 somites; n=7). Autofluorescence scans and vascular scans were obtained in the same fashion as for the C57Bl/6 embryos. Registration of the autofluorescence data produced a representative consensus average image of all embryo inputs as before, and we were similarly able to register the vascular scans of the embryos to produce a representative consensus average image, and thus register the vascular maps in 3D to a high degree (data not shown). The genetic background of mice, therefore, does not appear to have any bearing on whether or not registration of their anatomy or vascular trees is possible.

Side-by-Side Embryo Visualization and Registration Evaluation

Registration of seven 20- to 23-somite C57Bl/6 or CD-1 embryos enables us to analyze the functional and relevant 3D data that the registration pipeline provides. To visualize this, two 21-somite embryos from the C57Bl/6 registration pipeline are shown side by side in Figure 4A–E, and two 21-somite embryos from the CD-1 registration pipeline are shown side-by-side in Figure 4F–J. Figure 4A and F are representative autofluorescence coronal/frontal slices through the two embryos (one embryo in red, the other in green, along with their corresponding overlap image) of C57Bl/6 and CD-1 embryo pairs, respectively. Figure 4B and G are the corresponding PECAM-1 images of the same slices through the same embryos. Figure 4C and H are representative autofluorescence sagittal slices through two embryos (again, the first embryo depicted in red, the second in green, along with their corresponding overlap image) of the two C57Bl/6 and CD-1 embryo pairs, respectively, while Figure 4D and I are the corresponding PECAM-1 images of the same slices through the embryos. For presentation here, each image is actually a 5-slice stack in the selected plane (thus corresponding to a 27.5-μm slab), in order to better represent the structures of the anatomical organs and the blood vessels of the embryos. What is apparent from the autofluorescence data is that the head, and structures within the heart such as the atrioventricular canal, register together to a high degree. Looking closely at the registered vascular data, findings are similar in that blood vessels in the head region, intersomitic regions, dorsal aorta, and the endocardium in the

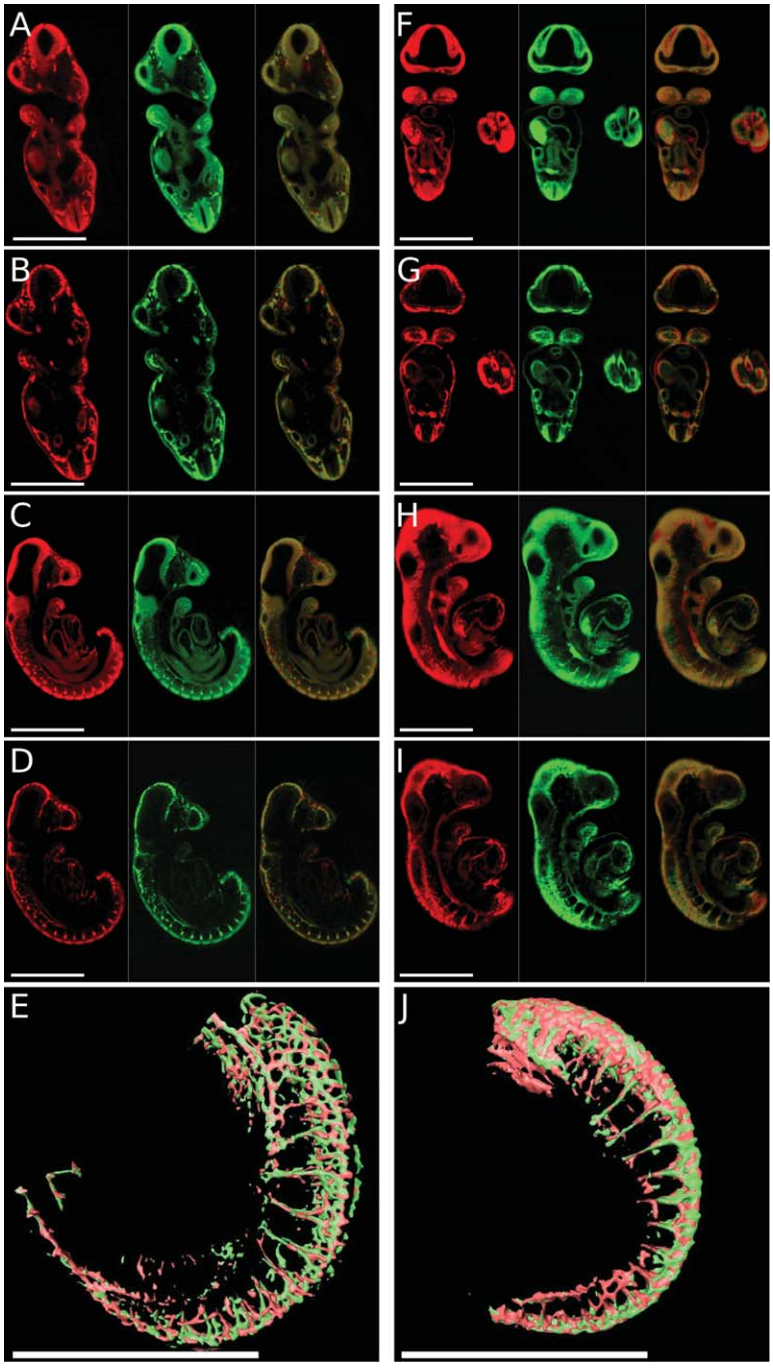

Fig. 4.

Fig. 4. Side-by-side embryo visualization and registration evaluation. Following registration of the seven E9.5 C57Bl/6 embryos and CD-1 embryos, respectively, the degree of overlap can be visualized in any desired plane in three-dimensional space. Two 21-somite embryos are shown side-by-side for each mouse strain, and have a high degree of overlap as shown by the representative coronal/frontal and sagittal sections. **A,B:** A representative coronal slice of the autofluorescence data (A) and the corresponding vascular data (B) of one 21-somite C57Bl/6 embryo (red, left), another 21-somite C57Bl/6 embryo (green, middle) alongside the overlap image of the two (right). **C,D:** A representative sagittal slice of the same two embryos, with the autofluorescence data depicted in C and the vascular data shown in D. The high degree of overlap is evident by the vast amount of yellow/orange colouring in the overlap image, even in heart structures such as the outflow tract and atrioventricular canal. When the anterior-most somites of the two embryos are segmented away from the right side and the rest of the body and isosurfaces generated, we see the high degree of overlap in a more three-dimensional fashion (**E**, viewed from the left side). Though the feeding vessels are not particularly patterned, the intersomitic vessels show a high degree of overlap following registration, and follow almost exact patterns at this stage of development. **F–J:** All images in F through J are representative of the CD-1 mouse strain, and are similarly presented as in A through E. Again, the high degree of overlap in is evident by the vast amount of yellow/orange colouring in the respective overlap images, and in the isosurface rendering of the vascular structures. All images in A–D and F–I are an average image of a 5-slice stack, thus creating a 27.5-μm slab of the data. Scale bars = 500 μm.

atrioventricular canals are registered to a high degree. In order to visualize the data in another fashion, surfaces can be rendered from the 3D dataset using an isosurface algorithm (using the visualization program Amira®, Visualization Sciences Group) that creates a digital surface corresponding to a selected intensity value threshold of the reconstructed data. Figure 4E and J illustrate the anterior-most intersomitic vessels of the left side of the body segmented away from the right side and from the rest of the embryo (for the C57Bl/6 and CD-1 embryo pairs, respectively) with the first embryo depicted in red and the second embryo depicted in green. What is clear is that the highly patterned intersomitic vessels are highly aligned in 3D space following registration, especially in these two cases where the two embryos are somite stage–matched. Although the feeding vessels of the developing somites have no discernible pattern, the intersomitic vessels themselves are precisely patterned and are highly conserved in mice that share identical genetic backgrounds.

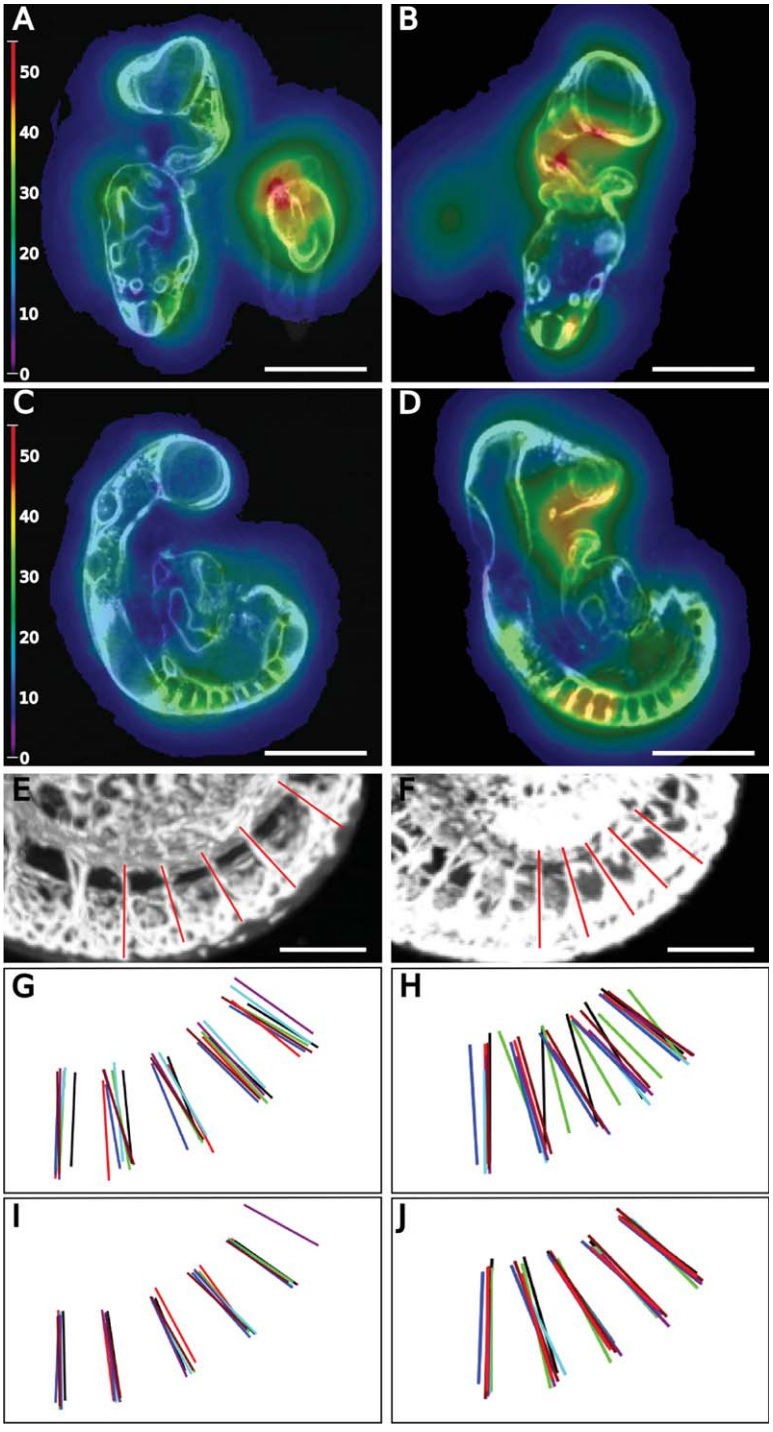

Fig. 5.

Vasculature Registration Evaluation

We next wanted to get a better understanding of how much our registration algorithm was changing the embryos in our pipeline in order to properly align their vascular maps following the initial gross anatomical alignment. The average vascular image, displayed in gray scale, can be overlaid with the average voxel displacement map for the entire collection of embryos in the pipeline, displayed as a heat map (Fig. 5A–D). This allows for the identification of

Fig. 5. Vasculature registration evaluation. To further evaluate the effectiveness of the vasculature registration algorithm, the average vascular tree data (grayscale) was overlaid with the average voxel displacement heatmap for the population data of the C57Bl/6 embryos (**A,C**, illustrating representative coronal and sagittal sections, respectively) and the CD-1 embryos (**B,D**). The heatmap scale bar (left side of A and C) displays the average voxel movement in all areas of the average embryo map (converted to μm). All data can be fully manipulated in 3D, and any slice can be viewed. The intersomitic vessels, which are highly aligned following registration, have undergone significant changes during registration as shown in C and D. In order to quantify this, maximum intensity projections (MIPs) through half each embryo was calculated in order to display the intersomitic vessels (**E,F**; representative MIPs of a C57Bl/6 and a CD-1 embryo, respectively). Centerlines were then manually drawn on the MIPs (red lines in E and F) for each embryo, and these were overlaid on top of one another both before (seven coloured lines in **G,H**) and after vasculature registration (**I,J**). The centerpoint of each line was then used to calculate the root mean squared (RMS) displacement of the intersomitic vessels. Prior to vascular registration, the average RMS displacement of the centerlines for the embryos was 32.73 μm for the C57Bl/6 vascular trees (G), and 56.21 μm for the CD-1 vascular trees (H). Following vascular registration, the RMS displacement was 17.28 μm for the C57Bl/6 intersomitic vessels (I), and 10.06 μm for the CD-1 intersomitic vessels (J). Scale bars = 500 μm (A–D) and 125 μm (E and F).

areas of both high similarity and dissimilarity, as it displays those voxels that have undergone large and small movements during the registration process. Figure 5A and C are representative coronal and sagittal sections from the C57Bl/6 registration pipeline, respectively, and Figure 5B and D are similar coronal and sagittal sections from the CD-1 registration pipeline. The voxel displacement maps display the exact regions in the registration volumes that have moved following registration, and to what degree (heat map scale bar has been converted to μm). What is evident is that, overall, the original registration of the vascular trees using the original autofluorescence deformation fields does not change too significantly with our additional non-linear registration steps, though certain areas do undergo fairly large realignment. There is a tightening of the blood vessel alignment throughout the vascular tree, particularly in the intersomitic vessel regions. In order to quantify the degree to which our vasculature registration more properly aligns the blood vessels, we decided to focus on the intersomitic vessel region of the embryos. Figure 5E and F are close-up maximum intensity projections (MIPs), through half of the embryo, of the middle of the intersomitic regions for a representative C57Bl/6 and CD-1 embryo, respectively. Overlaid on top of each MIP is a set of manually drawn centerlines corresponding to five sequential intersomitic blood vessels. This was done for all seven embryos in each pipeline, and the relative positions both before vascular registration (Fig. 5G and H) and after vascular registration (Fig. 5I and J) for both the C57Bl/6 and CD-1 registration pipelines are shown. In order to determine the relative positions of each intersomitic vessel, we next calculated the root mean square (RMS) displacement of the center point of each of the centerlines relative to one another in each of the intersomitic vessels. Prior to vascular registration, the average RMS displacement of the centerlines for the C57Bl/6 embryos was 6.00 voxels (32.73 μm) (Fig. 5G), and 7.28 voxels (56.21 μm) for the CD-1 vascular trees (Fig. 5H). Following vascular registration, the RMS displacement was 3.17 voxels (17.28 μm) for the C57Bl/6 vascular trees (Fig. 5I), and 1.30 voxels (10.06 μm) for the CD-1 vascular trees (Fig. 5J).

Vascular and Cardiovascular Developmental Differences at Sequential Developmental Stages

We next wanted to identify the useful information the registration algorithm was able to provide with respect to early developmental biology. As such, following registration, we looked at embryos side-by-side that differed in developmental stage by one or, at most, two somites for both the C57Bl/6 and the CD-1 embryos. Small developmental differences were detected, even though a difference of a few somites corresponds to only a few hours of gestational time. Figure 6A depicts slices of the registered vascular data of two C57Bl/6 embryos: a 23-somite embryo (left), a 21-somite embryo (middle), and the overlap of the two vascular maps (right), all shown in sagittal views (all images are depicted as an average of five slices through-plane, creating a 27.5-μm slab). When superimposed, the presence of an additional intersomitic vessel can be detected in the vascular tree of the 23-somite embryo (arrow), even though all other intersomitic vessels have been aligned to a high degree. Similarly, when we examine the intersomitic regions of the same 23-somite C57Bl/6 embryo (Fig. 6B, left) and a different 21-somite C57Bl/6 embryo (Fig. 6B, middle), once again the presence of an additional intersomitic vessel can be detected in the vascular tree of the 23-somite embryo that is not accounted for in the 21-somite embryo (arrow). Similarly, small developmental differences can be detected in the CD-1 strain of mice. Figure 6C is a representation of a 23-somite CD-1 embryo (left), a 22-somite embryo (middle), and the overlap of the two vascular maps (right; all images are depicted as an average of five slices through plane, creating a 27.5-μm slab). Once again, there is an obvious mis-match in the intersomitic region, where two intersomitic blood vessels from the 22-somite embryo cannot be aligned with the three intersomitic blood vessels from the 23-somite embryo (bracket in overlap image), even though the rest of the intersomitic vessels have been registered to a high degree.

At this same stage of development, the mouse heart is undergoing rightward looping (Srivastava and Olson, 2000), and trabeculations from the endocardium begin to form in the ventricle. When we examined the endocardial region of the C57Bl/6 embryos, we noted some small developmental differences between the registered datasets. Specifically, when the registered vascular maps of a 23-somite embryo (Fig. 7A and B, left) and a 20-somite embryo (Fig. 7A and B, middle) are examined side-by-side, a higher abundance of ventricular trabeculations in the heart of the 23-somite embryo (arrows in overlap image, right side) are evident, even though much of the rest of the heart (such as the endocardial cushion region) is highly aligned (Fig. 7A and B represent two different sagittal slices through the hearts of the embryos, and all images are an average of five slices through plane, creating a 27.5-μm slab). This suggests that rapid heart development/maturation is occurring in C57Bl/6 embryos at this point, and that such developmental differences can be captured by OPT. No such differences were detectable in the CD-1 population of mice at this stage of development; all embryos imaged had abundant and almost complete ventricular trabeculation patterns.

The presence of additional intersomitic blood vessels and an increase in ventricular trabeculation patterning illustrates the fact that small but detectable developmental maturation steps can be imaged and detected at early developmental time points. These small developmental landmarks would otherwise be difficult to detect without directly comparable images from 3D registration.

DISCUSSION

Presented here is a novel method in which early developmental processes can be tracked and visualized in their native three-dimensional space so that questions of scale and spatial

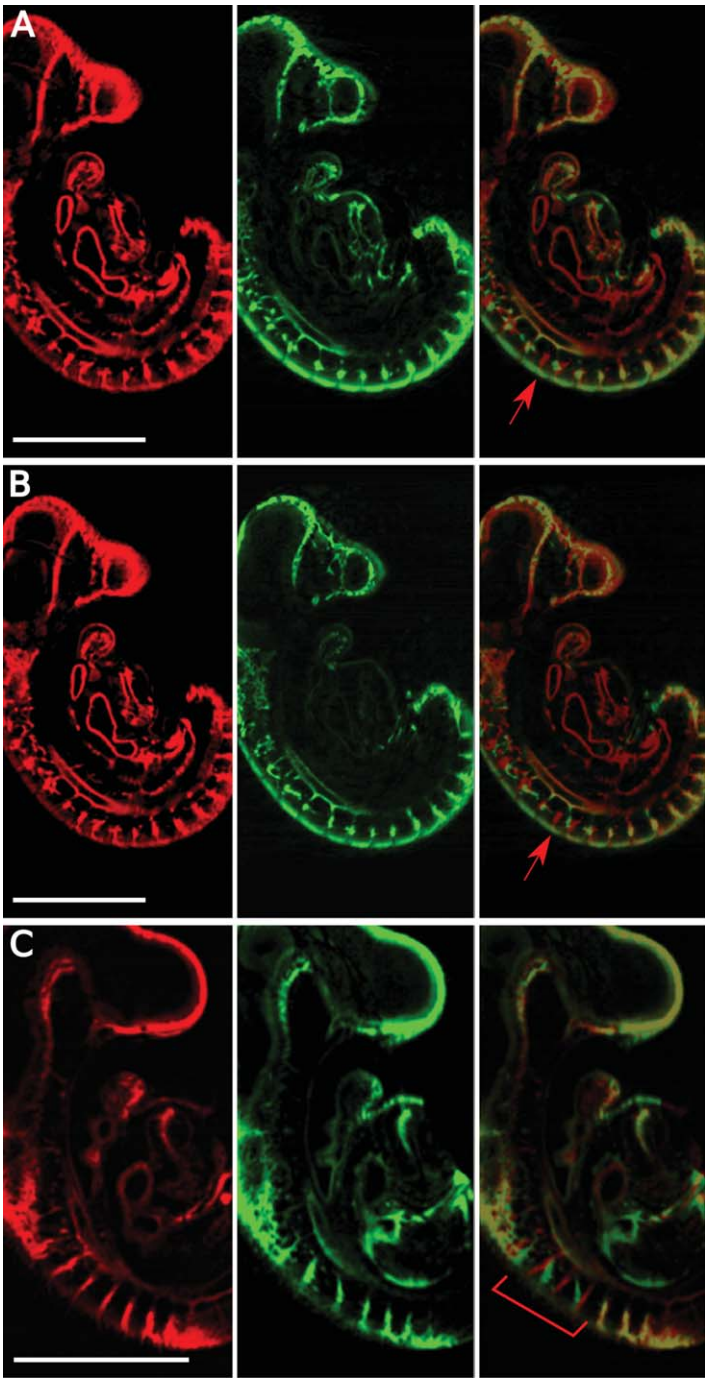

Fig. 6. Vascular differences are discernible at different temporal developmental stages. Following registration, small but discernible differences were noticeable in the vascular maps of both the C57Bl/6 and CD-1 embryos, most notably in the highly conserved and patterned intersomitic regions of the developing embryos. **A:** A representative sagittal section of the intersomitic region of one C57Bl/6 23-somite embryo (red, left), and another C57Bl/6 21-somite embryo (green, middle), alongside the overlap image (right). While most of the intersomitic vessels are highly registered, it is easy to spot one intersomitic vessel (arrow) from the 23-somite embryo that cannot be accounted for in the 21-somite embryo. **B:** Illustrates this point further, when the same 23-somite embryo (red, left) is visualized alongside a different 21-somite C57Bl/6 embryo (green, middle) and the overlap image (right) is examined. Again, while all intersomitic vessels are highly aligned, there is one vessel that is present in the 23-somite embryo that is unaccounted for in the 21-somite embryo (arrow). A similar story is evident when CD-1 embryos are analyzed side-by-side. **C:** One 23-somite CD-1 embryo (red, left), another 22-somite CD-1 embryo (green, middle), alongside the overlap image of the two (right). While the rest of the intersomitic vessels are highly aligned, there is a region present (bracket) where two vessels from the 22-somite embryo are attempting to align with three vessels from the 23-somite embryo. All images are an average image of a 5-slice stack, thus creating a 27.5-μm slab of the data. Scale bars = 500 μm.

orientation are no longer a confounding issue. The development of the cardiovascular system is an extremely complex process that has been studied extensively, in many animal model systems. Until now, however, it has not been possible to determine how similar the vascular structures of genetically identical mouse embryos are, and, conversely, how dissimilar these respective vasculatures can be when separated by only a few hours of developmental gestation. By systematically generating vascular maps of early mouse embryos at fixed developmental time points and registering these maps to littermate controls, it is now possible to observe the amount of change and strict patterning that occurs in the cardiovascular system over short time intervals. Here we chose to focus on embryos that were somite-stage matched at 20 to 23 somites, but previous work from our lab has shown that embryos up to 30 somites in development are amenable to PECAM-1 staining and OPT visualization (Walls et al., 2008). Unpublished results from our lab suggest that embryos up to 35 somites of development can be imaged using OPT, after which light scattering becomes a confounding issue as the tissue becomes too dense to be cleared effectively.

In the embryo proper, the formation of the major blood vessels and the developing heart is a tightly controlled and hierarchal process, which is why 3D cardiovascular maps generated by OPT are so amenable to registration. However, the blood vessels that arise in the extraembryonic tissues such as the developing yolk sac, though developing an arborized hierarchy of structures, are not stereotypically patterned. As such, any attempt to register the yolk sac vasculatures of multiple mouse embryos fails. Though mutations that affect the cardiovascular system in the embryo will often also have a negative effect on the yolk sac vasculature (Tanaka et al., 1999; Wakimoto et al., 2000; Huang et al., 2003; May et al., 2004), these developmental processes cannot be investigated using registration-based techniques.

The ability to register comparative multiple mouse embryos that have been imaged by OPT is a major

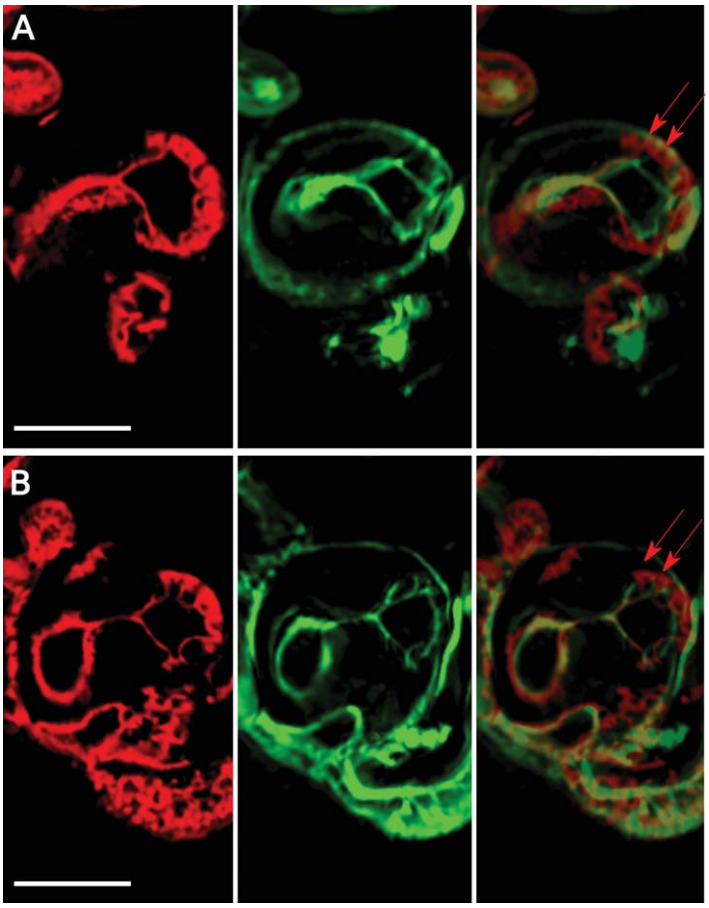

Fig. 7. Cardiac differences are discernible at different temporal developmental stages. Following registration, small but discernible cardiac maturation differences were observed in the C57Bl/6 strain of mice. Looking at two different sagittal slices through the developing hearts of a 23-somite embryo (**A,B**, left) and a 20-somite embryo (A, B, middle), the developing ventricle of the 23-somite embryo has significantly more ventricular trabeculations than the 20-somite embryo which is very noticeable in the overlapped image (arrows in A and B, right), even though the rest of the heart, including the endocardial cushions, is highly aligned. All images are an average image of a 5-slice stack, thus creating a 27.5-μm slab of the data. Scale bars = 250 μm.

advance in quantitative 3D imaging: to date only brains and embryos imaged by MRI or micro-CT have been amenable to this process (Spring et al., 2007; Lerch et al., 2008; Zamyadi et al., 2010; Cleary et al., 2011; Wong et al., 2012b). Since OPT has a much higher resolution and a superior contrast to both MRI and micro-CT, it allows for the imaging of much younger and smaller embryos, and it allows for the capture of molecular-specific markers. As shown here, it is possible to image minor structural differences in the developing hearts and growing vasculatures of embryos that differ by only a couple of somites.

Genetic mutations that affect the developing cardiovascular system have manifestations that may present earlier than previously appreciated, and may go unnoticed by conventional molecular biology techniques. Thus, there are many additional applications of this method. By using this newly developed registration process and comparing mutant models of vascular disease to wild-type controls, it will be possible in the future to pinpoint the critical time of expression of mutations by visualizing very specific differences in the comparative vascular maps that are generated. This will allow for a more specific, accurate, and quantifiable description of mouse models of cardiovascular disease. As well, this method need not be confined to the study of the cardiovascular system, nor to mouse models themselves. Presented here is a method that is very robust, and could be applied to diverse areas of scientific research, from mammalian limb development to zebrafish vascular development.

EXPERIMENTAL PROCEDURES

Mouse Lines

Both the C57Bl/6 and CD-1 mice were purchased from the isolator-raised, elite colony at Charles River (Wilmington, MA). Upon arrival at our mouse facility, following an extensive three-day health check in a full barrier, limited access conditioning room, the mice are housed in Tecniplast Greenline sterile ventilated caging with access to automated watering (acidified/RO/UV treated) and are fed irradiated Teklad 2918x extruded diet (Harlan Laboratories, Indianapolis, IN). In order to ensure genetic homogeneity in the mouse populations, the breeding colonies are only bred for three generations and all breeding cages are replenished with new stock from Charles River at the end of the three-generation cycle.

Embryo Collection and Staining

All embryos were collected and stained as described previously (Walls et al., 2008). Briefly, wild-type C57Bl/6 or CD-1 embryos were collected at embryonic day (E) 9.25–9.5 (20–23 somites). Noon of the day of vaginal plugging was considered to be E0.5. Embryos were dissected and fixed in 4% paraformaldehyde for 2 hr. Endogenous peroxidase activity was quenched by immersing the embryos in 3% H_2O_2, and non-specific antibody staining was blocked by pre-incubating embryos in 1% heat-inactivated fetal calf serum (FCS) and 1% normal goat serum. Embryos were then stained overnight with 5 μg/mL anti-PECAM-1 antibody (Mec13.3) (BD Pharmingen, San Jose, CA). The primary antibody was then detected by incubating the embryos overnight with an anti-rat horseradish peroxidase (HRP) secondary antibody (BioSource, Grand Island, NY), followed by incubation with a tyramide-Cy3 reagent (1:50; Perkin-Elmer, Waltham, MA) for 1 hr. The secondary antibody was then washed away with Tris-

NaCl-Triton X-100 (TNT) buffer overnight. All animal experiments were approved by the Animal Care Committee at Mount Sinai Hospital (Toronto, ON), and were conducted in accordance with guidelines developed by the Canadian Council on Animal Care.

Optical Projection Tomography (OPT) of Embryos

Optical projection tomography was performed as described previously (Walls et al., 2007). The OPT microscope was home built (Wong et al., 2012a) to provide a good optical spatial resolution of ~6 μm, a large solid angle, robust components for stability, and a large sample holder for specimens. Briefly, specimens were embedded in 1% low melting point agarose and subsequently cleared using a 1:2 mixture of benzyl alcohol and benzyl benzoate (BABB). The embryos were then suspended from a stepper motor and immersed in an optically flat cuvette containing BABB. Images of the specimen were formed using a Qioptiq Telecentric Zoom 100 microscope equipped with a 0.5× Optem objective lens. The zoom setting used for image formation resulted in a numerical aperture of 0.05. Images were acquired with a Qimaging Retiga 4000DC CCD camera with pixel size equal to 7.4 μm/pixel. Light from a mercury lamp was directed onto the specimen and filter sets were used to created fluorescent images of the specimen. An autofluorescence view was captured with a GFP excitation filter set in the illumination and detection light path, and a view of the PECAM-1 fluorescence from the specimen was captured using a Cy3 excitation filter set in the illumination and detection light path. The sample was rotated stepwise with a 0.3-degree step size through a complete revolution and views were acquired at each step. The acquisition time for a single filter set is approximately 20 min (Wong et al., 2012a).

Reconstruction of OPT Data

Each OPT image approximates a parallel ray projection through the embryo. As subsequent images are acquired from the CCD, a sinogram is formed, which is then used to reconstruct the corresponding slice through the embryo using the standard convolution filtered back-projection algorithm (Slaney and Kak, 1988). The reconstruction of all slices produces a 3D volumetric representation of the embryo with isotropic pixel size of 4.45 μm. The resulting 3D reconstruction of autofluorescence images and its corresponding 3D reconstruction of Cy3 images are co-registered. The datasets are typically on the order of 2.0 GB in size.

3D Registration of Embryos

Autofluorescence scans of all embryos used for the registration were first subjected to a rigid body alignment [3 rotations, 3 translations (1 in each of the x, y, z directions)] to orient the embryos into a preliminary atlas. This step removes postural and angular discrepancies. Next, all possible pair-wise 12-parameter affine transformations (3 scales, 3 shears, 3 rotations, and 3 translations) were computed, and a transform to an unbiased aggregate was created for each individual embryo. All scans were then averaged to create the first population average, which represents the average anatomy of the embryos after accounting for overall differences in body orientation and size. Next, an iterative 6-generation multi-scale, non-linear alignment procedure was computed, initially registering each embryo towards the 12-parameter registration atlas, and subsequently towards the atlas of the previous nonlinear generation. Each step involves detailed matching of anatomical features using a coarse grid that becomes progressively finer with each non-linear step, finally ending at the resolution of the imaging voxels. All registrations were performed using the MNI autoreg tools (Collins et al., 1994). The end result places all autofluorescence scans into precise alignment with each other in an unbiased manner. Evaluation by cross-correlation analysis revealed that for the C57Bl/6 embryos, the cross-correlation coefficient for the autofluorescence data was 0.79 ± 0.01 (indicating a 79% overlap of all voxels, $\pm$ the standard error of the mean), while for the CD-1 embryos, the cross-correlation coefficient for the autofluorescence data was 0.86 ± 0.02. The deformation field for each individual embryo, which contains all information pertaining to the functions performed on it, was then applied to each embryo's respective vasculature scan, thus approximately aligning all vasculature scans of the embryos with their autofluorescence scan counterparts. At this point the cross-correlation coefficient for the C57Bl/6 embryos was 0.55 ± 0.01, while for the CD-1 embryos the cross-correlation coefficient was 0.65 ± 0.02. In order to account for any residual inconsistencies in alignment at this stage (since the vasculature has a very fine resolution), and to more precisely align the vascular trees, the vasculature scans were put through another iterative 6-generation multi-scale, non-linear alignment procedure as before (matching of vascular features using a coarse grid that becomes progressively finer with each non-linear step, finally ending at the resolution of the imaging voxels). Thus, all vascular scans are placed into precise alignment with each other in an unbiased fashion. Evaluation by cross-correlation analysis revealed that for the C57Bl/6 embryos the cross-correlation coefficient for the vascular data was 0.69 ± 0.02 following registration, while for the CD-1 embryos, the cross-correlation coefficient following registration was 0.80 ± 0.01.

ACKNOWLEDGMENTS

G.A.A. is a recipient of an Ontario Graduate Scholarship. R.M.H. is a Canada Research Chair in Imaging Technologies in Human Disease and Preclinical Models. The authors gratefully acknowledge funding for the Ontario Preclinical Imaging Consortium from the Ontario Research Fund.

REFERENCES

Chaturvedi K, Sarkar DK. 2006. Isolation and characterization of rat pituitary endothelial cells. Neuroendocrinology 83:387–393.

Cleary JO, Modat M, Norris FC, Price AN, Jayakody SA, Martinez-Barbera JP, Greene ND, Hawkes DJ, Ordidge RJ, Scambler PJ, Ourselin S, Lythgoe

MF. 2011. Magnetic resonance virtual histology for embryos: 3D atlases for automated high-throughput phenotyping. NeuroImage 54:769–778.

Coffin JD, Poole TJ. 1988. Embryonic vascular development: immunohistochemical identification of the origin and subsequent morphogenesis of the major vessel primordia in quail embryos. Development 102:735–748.

Collins DL, Neelin P, Peters TM, Evans AC. 1994. Automatic 3D intersubject registration of MR volumetric data in standardized Talairach space. J Comput Assist Tomogr 18:192–205.

Dorr AE, Lerch JP, Spring S, Kabani N, Henkelman RM. 2008. High resolution three-dimensional brain atlas using an average magnetic resonance image of 40 adult C57Bl/6J mice. NeuroImage 42:60–69.

Drake CJ, Fleming PA. 2000. Vasculogenesis in the day 6.5 to 9.5 mouse embryo. Blood 95:1671–1679.

Gerety SS, Anderson DJ. 2002. Cardiovascular ephrinB2 function is essential for embryonic angiogenesis. Development 129:1397–1410.

Huang C, Sheikh F, Hollander M, Cai C, Becker D, Chu PH, Evans S, Chen J. 2003. Embryonic atrial function is essential for mouse embryogenesis, cardiac morphogenesis and angiogenesis. Development 130:6111–6119.

Isogai S, Horiguchi M, Weinstein BM. 2001. The vascular anatomy of the developing zebrafish: an atlas of embryonic and early larval development. Dev Biol 230:278–301.

Isogai S, Lawson ND, Torrealday S, Horiguchi M, Weinstein BM. 2003. Angiogenic network formation in the developing vertebrate trunk. Development 130:5281–5290.

Kovacevic N, Henderson JT, Chan E, Lifshitz N, Bishop J, Evans AC, Henkelman RM, Chen XJ. 2005. A three-dimensional MRI atlas of the mouse brain with estimates of the average and variability. Cereb Cortex 15:639–645.

Lerch JP, Carroll JB, Dorr A, Spring S, Evans AC, Hayden MR, Sled JG, Henkelman RM. 2008. Cortical thickness measured from MRI in the YAC128 mouse model of Huntington's disease. NeuroImage 41:243–251.

Lickert H, Takeuchi JK, Von Both I, Walls JR, McAuliffe F, Adamson SL, Henkelman RM, Wrana JL, Rossant J, Bruneau BG. 2004. Baf60c is essential for function of BAF chromatin remodelling complexes in heart development. Nature 432:107–112.

May SR, Stewart NJ, Chang W, Peterson AS. 2004. A Titin mutation defines roles for circulation in endothelial morphogenesis. Dev Biol 270:31–46.

Peng H, Chung P, Long F, Qu L, Jenett A, Seeds AM, Myers EW, Simpson JH. 2011. BrainAligner: 3D registration atlases of Drosophila brains. Nat Methods 8:493–500.

Poole TJ, Coffin JD. 1989. Vasculogenesis and angiogenesis: two distinct morphogenetic mechanisms establish embryonic vascular pattern. J Exp Zool 251:224–231.

Sharpe J, Ahlgren U, Perry P, Hill B, Ross A, Hecksher-Sorensen J, Baldock R, Davidson D. 2002. Optical projection tomography as a tool for 3D microscopy and gene expression studies. Science 296:541–545.

Slaney M, Kak AC. 1988. Principles of computerized tomographic imaging. IEEE Press. New York.

Spring S, Lerch JP, Henkelman RM. 2007. Sexual dimorphism revealed in the structure of the mouse brain using three-dimensional magnetic resonance imaging. NeuroImage 35:1424–1433.

Srivastava D, Olson EN. 2000. A genetic blueprint for cardiac development. Nature 407:221–226.

Suchting S, Freitas C, le Noble F, Benedito R, Breant C, Duarte A, Eichmann A. 2007. The Notch ligand Delta-like 4 negatively regulates endothelial tip cell formation and vessel branching. Proc Natl Acad Sci USA 104:3225–3230.

Tanaka M, Chen Z, Bartunkova S, Yamasaki N, Izumo S. 1999. The cardiac homeobox gene Csx/Nkx2.5 lies genetically upstream of multiple genes essential for heart development. Development 126:1269–1280.

Wakimoto K, Kobayashi K, Kuro OM, Yao A, Iwamoto T, Yanaka N, Kita S, Nishida A, Azuma S, Toyoda Y, Omori K, Imahie H, Oka T, Kudoh S, Kohmoto O, Yazaki Y, Shigekawa M, Imai Y, Nabeshima Y, Komuro I. 2000. Targeted disruption of Na+/Ca2+ exchanger gene leads to cardiomyocyte apoptosis and defects in heartbeat. J Biol Chem 275:36991–36998.

Walls JR, Sled JG, Sharpe J, Henkelman RM. 2007. Resolution improvement in emission optical projection tomography. Phys Med Biol 52:2775–2790.

Walls JR, Coultas L, Rossant J, Henkelman RM. 2008. Three-dimensional analysis of vascular development in the mouse embryo. PLoS ONE 3:e2853.

Wong MD, Dazai J, Walls JR, Henkelman RM. 2012a. Design and implementation of a custom built optical projection tomography system. In preparation.

Wong MD, Dorr AE, Walls JR, Lerch JP, Henkelman RM. 2012b. A novel 3D mouse embryo atlas based on micro-CT. Development 139:3248–3256.

Zamyadi M, Baghdadi L, Lerch JP, Bhattacharya S, Schneider JE, Henkelman RM, Sled JG. 2010. Mouse embryonic phenotyping by morphometric analysis of MR images. Physiol Genomics 42A: 89–95.

Developmental Dynamics